Analysis of the variability of African easterly waves in simulations with ARPEGE-Climat

Jean-François Royer, Fabrice Chauvin and Hervé Douville

Météo-France/CNRM, 42 Avenue Coriolis 31057 Toulouse Cedex 01, France
Jean-francois.Royer@meteo.fr

Abstract

Intraseasonal and interannual variability of African Easterly Waves (AEW) are assessed by means of Spatio-Temporal Spectral Analysis (STSA) and Complex Empirical Orthogonal Functions (CEOF). These methods are applied to the reanalysis data ERA15 from ECMWF and to an ensemble simulation with 10 members performed with the Météo-France ARPEGE-Climat AGCM. The first CEOF amplitude captures an interannual variability of the AEW intensity and a latitudinal shift of their tracks, which for the simulations is correlated to temperature anomalies in the tropical Atlantic. The temporal structure of the CEOF shows a seasonal cycle in wave activity, with august maximum in August, together with strong intraseasonal modulation of their amplitude. A spectral analysis of the intraseasonal variability shows that the first CEOF selects low-frequency fluctuations with periods longer than 20 days, while the second EOF has mostly a broad maximum over 5 to 10 days. The selection of low-frequency intraseasonal variations by CEOF-1 is a useful feature for the studying the relationship of AEW with the large-scale evolution of the West African monsoon and possibly with the MJO.

1. Introduction

Fluctuations of the West African Monsoon and the associated interannual rainfall variability are of great importance for the agriculture and economy of West African countries. West African climate is influenced by westward propagating synoptic scale instabilities, known as African Easterly Waves (AEWs). Usual characteristics of AEWs are a period of 3 to 5 days and an associated wavelength from 2000 to 4000 km (Burpee 1972, Reed *et al.* 1977). A second regime has been discovered, corresponding to a 6 to 9 day periodicity and a 6000 km wavelength (Diedhiou *et al.* 1998, 1999). AEWs occur during the monsoon season from June to September, with a maximum in August. The predictability of AEW intensity and location is important for seasonal prediction of both West African precipitation, and hurricane activity over the Atlantic. AEWs have been studied in simulations with Atmospheric General Circulation Models (GCMs) (Estoque et al., 1983; Druyan and Hall, 1994; Thorncroft and Rowell, 1998; Ceron and Gueremy, 1999; Fyfe, 1999). Using a space–time spectral analysis and a complex empirical orthogonal function (CEOF) analysis applied to the 850 hPa vorticity, Ceron and Gueremy (1999) (hereafter CG99) have examined the ability of the the former Meteo-France AGCM (Emeraude) at T42 resolution, at simulating the space-time variability of AEWs as identified in ECMWF analyses. They found that waves in the GCM propagate more slowly than those from the ECMWF analyses, while the location, intensity, barotropic and baroclinic energy conversions were consistent. When decomposing the variance in the 2.5-6 day bandwidth with a Complex Empirical Orthogonal Function (CEOF) method, they identified two main modes: a ``northern single-track'' mode (located between 15°N and 20°N over land) and a ``dual-track'' mode (with a first maximum located between 18°N and 25°N over land and a second located around 10°N over the Atlantic). In a subsequent study (Céron et al, 2001) (hereafter CGS01) they used the ARPEGE-Climat GCMl, a larger sample of years from the reanalysis and applied varimax rotation to the CEOFs to separate more clearly a “Northern and continental”

mode from a "Southern and oceanic" one. Moustaoui *et al*. (2002) have tested a more recent variable resolution version of the ARPEGE-Climat GCM with a stretched-grid centered over the Gulf of Guinea, and have shown, by means of a Local Mode Analysis (Goulet and Duvel 2000), that it was able to reproduce the variance associated with AEW and its seasonal evolution.

The purpose of the present study is to extend the previous studies on the characteristics of AEWs with the latest version of the GCM ARPEGE-Climat, and with an ensemble of simulations, in order to better assess the stability and statistical significance of the results, and the potential predictability of intraseasonal and interannual variability of AEW over Africa. The model and experiments are described in section 2, as well as the statistical methods used for the analysis of AEWs activity. The spatial patterns of the modes are presented in section 3. The interannual variability of the modes is studied in section 4, and their intraseasonal fluctuations in section 5. Conclusions are given in section 6.

2. Model, experiments and statistical tools

2.1. The ARPEGE/climat model

The simulations reported here have been performed with the ARPEGE-Climat atmospheric general circulation model (AGCM), an adaptation for climate simulations of the ARPEGE/IFS (Integrated Forecast System) numerical weather prediction model developed jointly by Météo-France and ECMWF. It is a spectral atmospheric model with a hybrid-pressure vertical coordinate. Since the first release of the ARPEGE-Climat model (Déqué *et al*., 1994), many developments have been included, both dynamical and physical. Here we use ARPEGE version 3 (Déqué *et al*., 1999) with a semi-lagrangian numerical integration scheme and a 30 minute time-step. The physical package includes the turbulence scheme of Louis *et al.* (1981), the statistical cloud scheme of Ricard and Royer (1993), and the mass-flux convective scheme with Kuo-type closure of Bougeault (1985). The radiative scheme is derived from Morcrette (1990) and is activated every 3 hours. More details about the physics can be found in Geleyn *et al*. (1995). In this study, the model is used with 31 vertical levels and a T63 triangular truncation. The linear Gaussian grid associated with this truncation is a 128 x 64 longitude-latitude grid, reduced by a poleward decrease in the number of longitudes outside the tropics. Over the continents, the ISBA (Interaction Soil Biosphere Atmosphere) land surface scheme (Noilhan and Planton, 1989) is used to provide boundary conditions for the computation of surface fluxes (Mahfouf *et al*., 1995). The land surface model (LSM) includes a 4-layer heat diffusion scheme, a more physical treatment of snow cover (Douville *et al*. 1995a and b) and deep drainage (Mahfouf and Noilhan 1996).

2.2. Design of the experiments

In this study, the ARPEGE-Climat AGCM is used to perform global simulations in which soil moisture is fully interactive. Each experiment consists of 10-member ensembles for each of the fifteen summer monsoon season from June to September (JJAS) from 1979 to 1993. All members for a specific year are forced by the same AMIP I (Gates 1992) observed monthly mean SST, and differ only in their initial conditions. ECMWF reanalyses (ERA15, Gibson *et al*. 1997) are used to initialise both the atmospheric and land surface variables on May 27 each year. For each season, the 10 members are generated by starting the model from slightly different initial conditions, produced by introducing random perturbations in the atmospheric prognostic variables. All members of a given season share the same land surface initial conditions. The experiment design is described in details by Douville (2003) who also performed similar simulations with a relaxation of soil moisture toward monthly mean conditions in order to study the importance of soil moisture feedbacks for seasonal predictability.

2.3. Methods of statistical analysis

In order to study intraseasonal variability of African Easterly Waves daily values of relative vorticity at 850 hPa were extracted from the simulations. The choice of this level was based on the previous study of Céron and Guérémy (CG99 and CGS01). A first aim of the present study is to check that ARPEGE-Climat is able to reproduce the results of these previous studies. Other studies have preferred to focus on the 700 hPa level where the African Easterly Jet is maximum and/or on the meridional wind instead of vorticity (Diedhiou *et al.* 1998, Fyfe 1999). Reed *et al.* (1977) have shown that both levels seem appropriate for the study of AEW.

In CG99, innovative statistical methods were used to assess space-time variability of AEW. These methods are based on a combination of Space-Time Spectral Analysis (STSA) (Hayashi, 1977, 1979 and 1982) and Complex Empirical Orthogonal Function (CEOF) analysis (Wallace and Dickinson, 1972). The two methods will be only briefly described hereafter. A more complete description can be found in CG99. The spatial domain chosen for this study is between 40°W and 40°E, 5°S and 34°N, and is covered by 29 and 14 longitude and latitude model grid points. The time-span considered is 123 days, corresponding to the June to September (JJAS) summer monsoon season.

2.4. Temporal spectral window of AEW

In order to assess the wavelength and frequency of AEW, STSA was adopted, based on the methodology developed by Hayashi (1977, 1979 and 1982) and extended in CG99. It consists of a space-time spectral Fourier decomposition of the dataset in both zonal and meridional directions, and a calculation of the cross-spectrum between the real and imaginary parts of the space spectral coefficients. A zonal space-time cross-spectrum is obtained by summing over all meridional wavenumbers,. This spectrum can be split in standing, eastward and westward waves. This methodology allows visualisation of AEW energy spectra in the spatio-temporal domain. Figure 1a shows mean propagative space-time spectra of relative vorticity at 850 hPa, averaged over the 15 seasons (JJAS) and the 10 members for each year. The horizontal axis is labelled in time harmonics (the number of times that AEW occur among the 123 days) with negative (positive) values representing a westward (eastward) propagation. The vertical axis is labelled in zonal harmonics (the number of grid points where AEW occur among the 29 longitudes in the domain). AEW variance is clearly seen in this figure with periods centred on 4.5 days (27.5 occurrences over 123 days) and wavelengths centred on approximately 2600 km (3.1 occurrences on 29 longitudes). Additional energy is also seen in the low frequency domains. This residual energy can be eliminated by filtering the initial raw data, so as to focus on the spectral domain of AEWs. This was done by applying a fourth-order Butterworth filter (Hamming, 1977) centred on the 3.5- to 6-day bandwidth. The results of the same STSA applied on the filtered dataset (Figure 1b) show the efficiency of the filter in selecting only the westward travelling AEWs.

3. Spatial patterns of the modes of variability of AEW

Two modes of variability for the relative vorticity at 850 hPa have been found by CG99 in the ECMWF reanalysis: a northern continental mode and a southern oceanic mode. The methodology used to separate the two modes was based on CEOF which is a particularly suitable method for the analysis of travelling phenomena (Wallace and Dickinson, 1972; Horel, 1984). The multi-year ensemble simulations make it possible to assess the stability and robustness of the model in simulating the different years. The CEOF analysis has been performed on each seasonal run (150 runs) and the first two modes identified in each of the runs have been aggregated into mean mode patterns (MMPs) for each year, and for the whole period. The first MMP (Figure 2a) shows a pattern with a maximum over West Africa centred at 15°N-8°W and a limited southwestward extension over the ocean. The second MMP (Figure 3b) shows two maxima over North Africa: the first located in the 10-15°N belt between 15°E and 30°E, corresponding to a region of AEW

generation and the second extending over West Africa with a maximum located at 17.5°N on the Greenwich meridian.

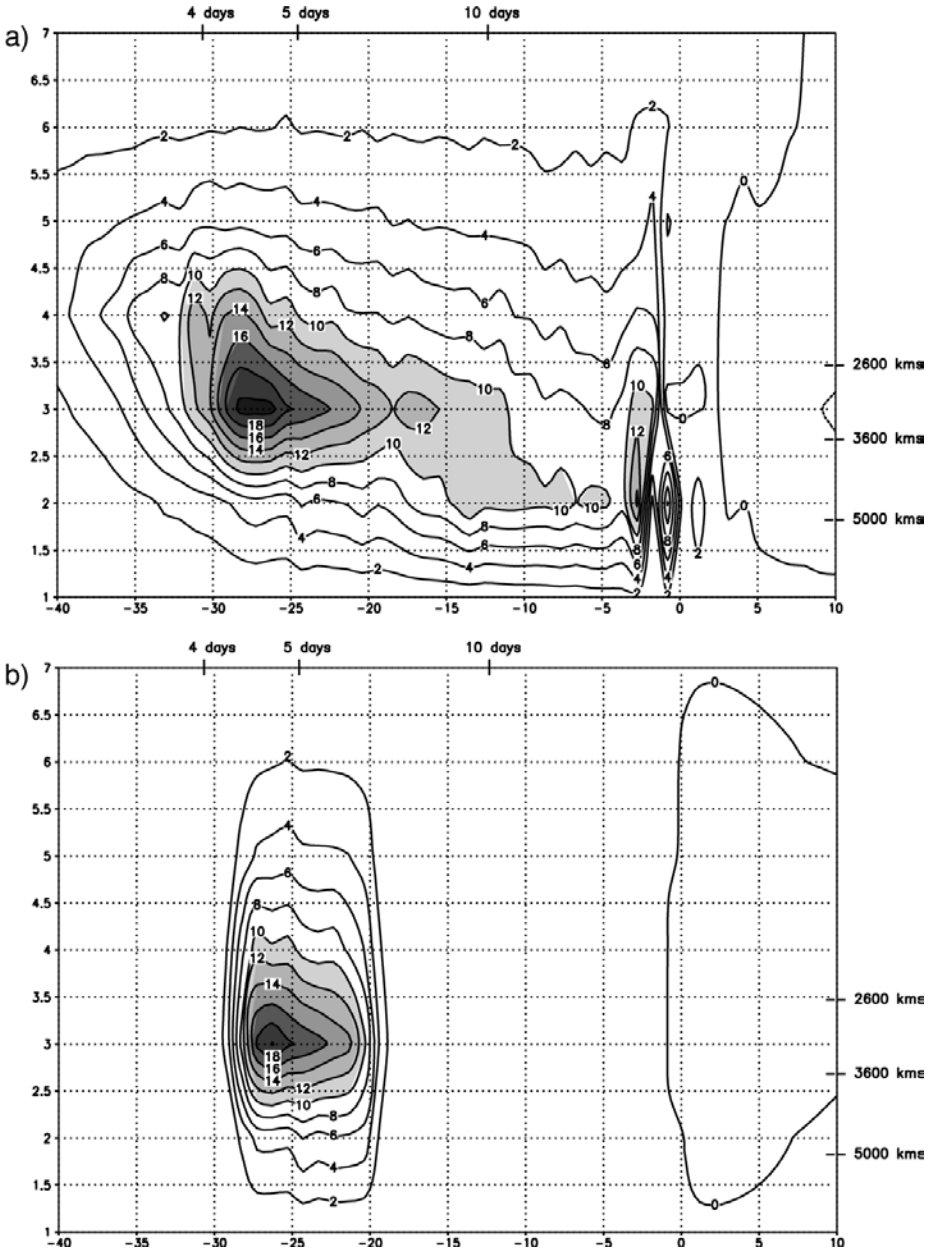

Figure 1: Mean propagative spatio-temporal spectra of GCM 850 hPa vorticity averaged over the 15 year 10-ensemble runs. a) raw data and b) data filtered in AEW temporal window. Contour interval: 2 x $10^{-15}s^{-2}$.

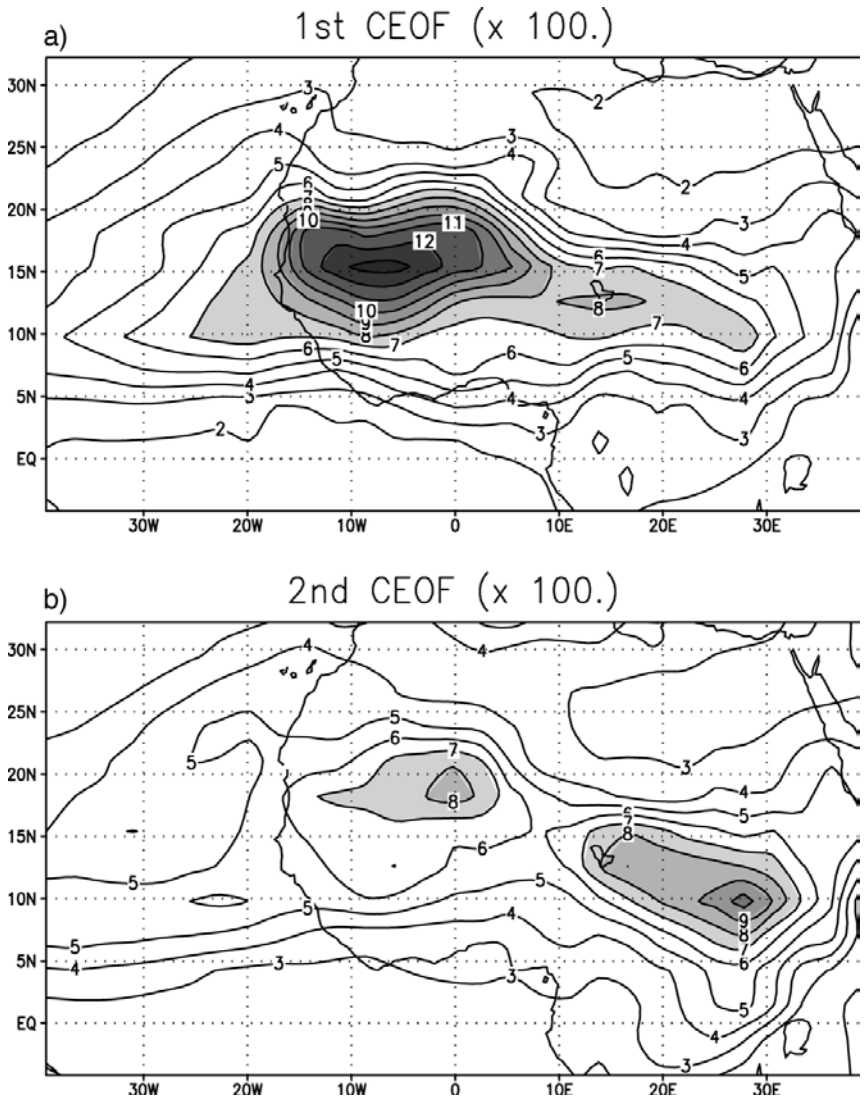

Figure 2: Mean amplitude of a) first CEOF and b) second CEOF of filtered GCM 850 hPa vorticity. Contour interval: 10^{-2}.

A large oceanic extension with a weaker intensity is also apparent. Thus, as in CG99, two modes with distinct patterns are clearly identified in the ARPEGE-Climat GCM, though their locations and patterns are not exactly the same as in the previous study. The mean explained variances of the first two CEOFs are respectively 37% and 17% with standard deviations of 6.7% and 2.6%. The first two modes obtained with the ECMWF 15-years reanalysis (25% and 16% with standard deviations of 2% and 1.3%), at the same resolution as the model, show similar patterns (Figure 3) with a sharper extension and maxima located approximately 3° further North compared with the GCM maxima. In addition, the first mode shows a local maximum over West African coast between 5°N and 10°N. Unlike the second mode in the GCM, the second mode in ECMWF reanalysis does not show much variance in the region of AEW generation. It means that the intensity of AEW is weak at the early stage of their life or that the 850 hPa vorticity fails at characterising the AEW during this period. Céron *et al.* (2001) already mentioned that the first two modes were not clearly separated in the ECMWF reanalysis and they applied a rotation of the CEOF to enhance the discrimination between the two modes. The CEOF patterns obtained in the simulations confirm the results of Moustaoui *et al.* (2002) concerning the ability of the ARPEGE-Climat GCM to represent the AEW quite realistically. The ability of the GCM to represent the interannual variability of the AEW is another question worth being investigated since it is of primary importance in some regions of West Africa that are strongly dependent on interannual variability of rainfall.

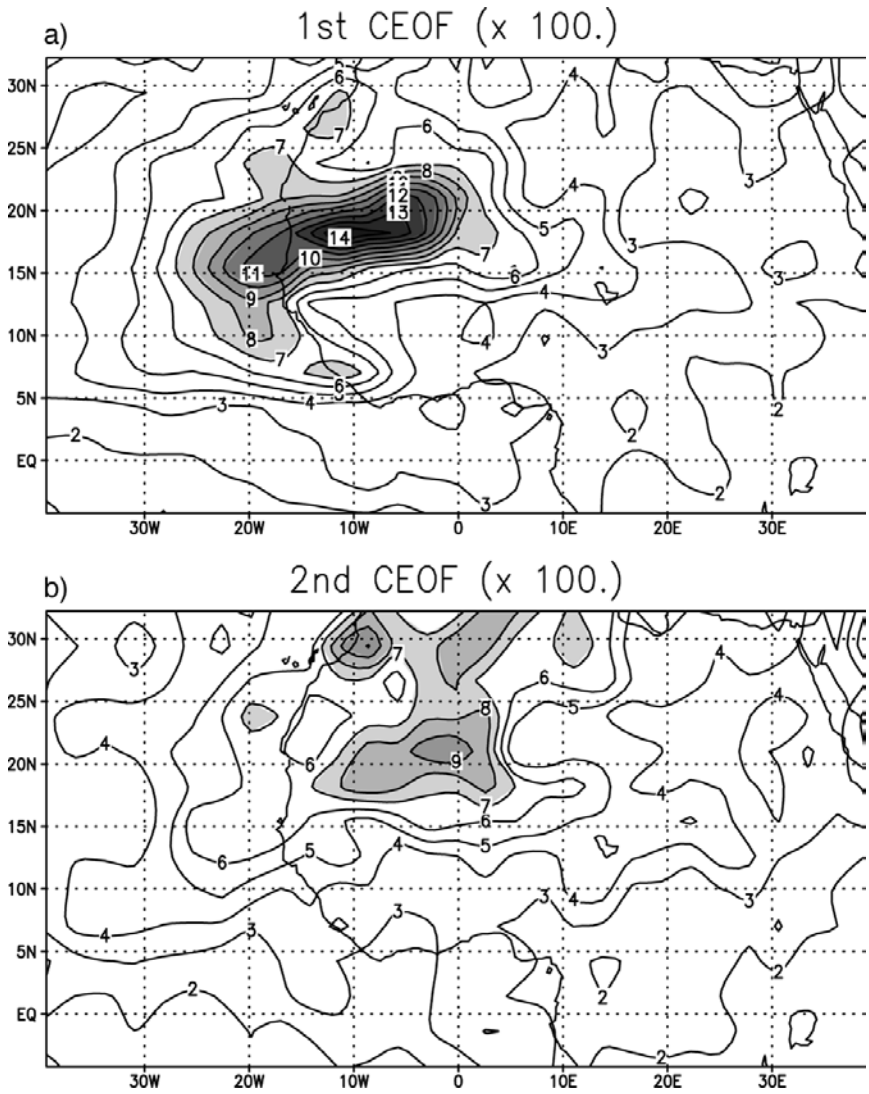

Figure 3: Same as Figure 2, but for the ECMWF 15-years reanalysis (1979-1993).

4. Interannual variability of the modes

Figure 4 shows interannual variability of the total variance explained, respectively, by the first and second modes (Figure 4a and Figure 4c). The mean periods are plotted on Figure 4b and 4d. Error bars represent one standard deviation on each side of the mean annual value (standard deviation is calculated with the 10 realisations of each seasonal value). Triangles pointing up and down are maximum and minimum of the ten realisations. Interannual variability is evident in Figure 4a and c, though the spread is relatively large. Higher variance years are 1979, 1984 and 1988, associated with a positive anomaly of the first MMP over the Guinea Coast region and a negative one over Sahel (Figure 6). Particularly low variances are observed in 1982, 1983, 1991, 1992 and 1993. These years are associated with a Sahelian positive and Guinean negative anomalies of the first MMP and are also characterised by a small dispersion of the total variance of the mode around its mean value. It can be seen from Figure 6 that such variations correspond to a dipolar pattern in the MMP anomaly, characterising a shift in the MMP, northward or southward according to the year. Thus, years 1983, 1991, 1992 and, to a lesser extent, 1993 are characteristic of a northward shift while years 1979, 1981, 1984 and 1988 are characteristic of a southward shift of the MMP.

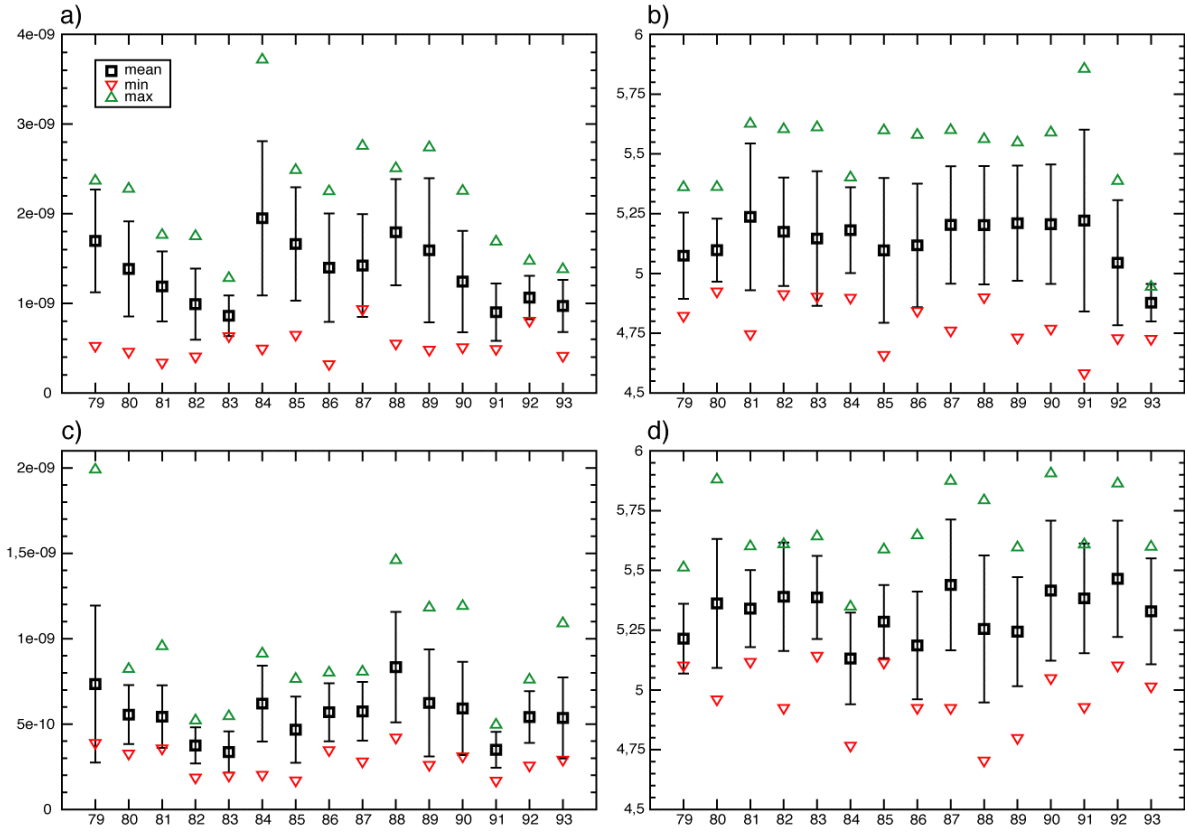

Figure 4: Interannual variability of 10-ensemble mean variances a)-c) and periods b)-d) of respectively first and second CEOF amplitude of GCM filtered 850 hPa vorticity. Bars represent one standard deviation on each side of the mean. Triangle pointing up and down are maximum and minimum of the 10 elements. Units are s^{-2} for a)-c) and days for b)-d).

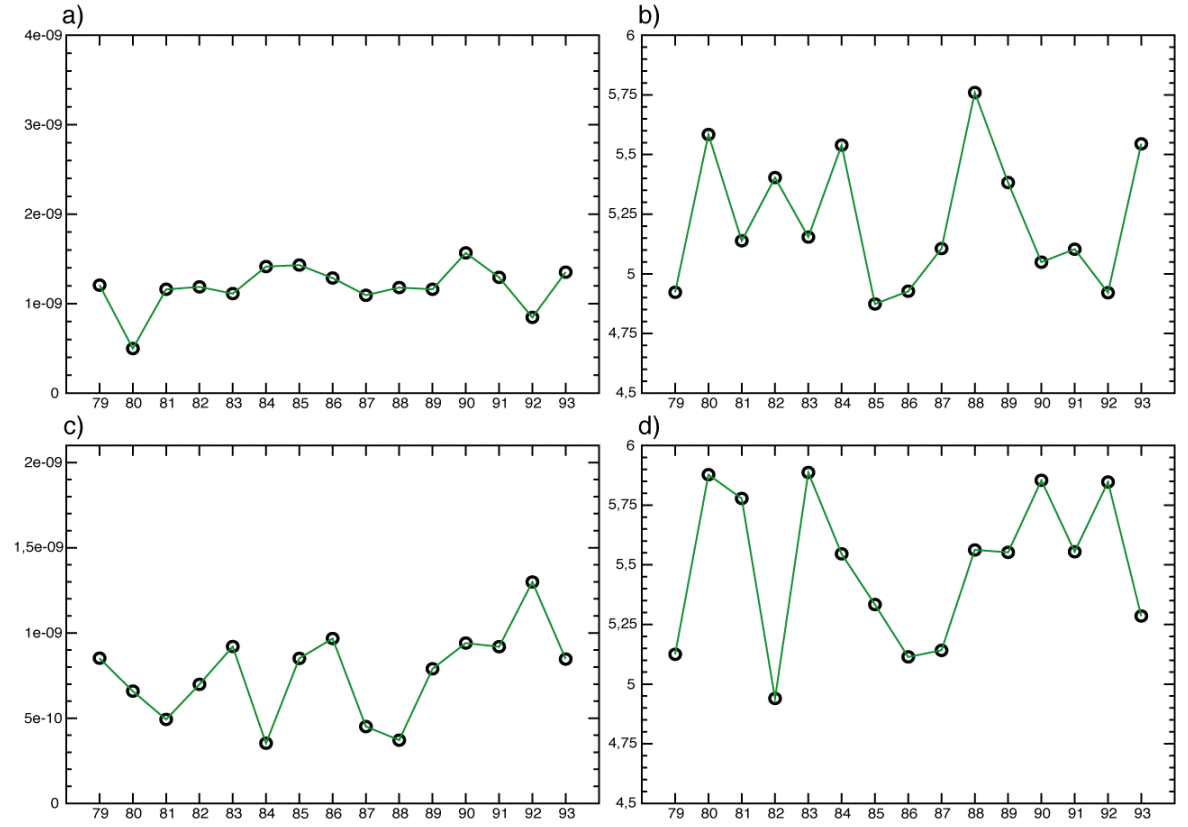

Figure 5: Interannual variability of variances a)-c) and periods b)-d) of respectively first and second CEOF amplitude of ERA15 filtered 850 hPa vorticity.

A dipolar structure also exists in the ECMWF reanalysis (not shown) except that the dipole is located further West compared with the GCM, between longitudes 10°W and 20°W. As a consequence, northward shifted years for ERA15 are not exactly the same as those for the GCM. Nevertheless, the dipolar structure does not seem to be unrealistic, particularly when considering that the MMP pattern in ERA15 extends more clearly over the West African coast (Figure 3) than in the GCM. Interannual variability of variances and periods of the first two MMPs of ECMWF reanalyses are presented in Figure 5. Variance of the first MMP shows a low interannual variability compared with that of the GCM. The second MMP shows some interannual variability but extreme years are not the same as those of the GCM. These discrepancies between model and reanalysis may be explained by a different repartition of explained variance between the different modes of both. Then, even if the dominant mode of the reanalysis is somewhat different from that of the GCM, some similarities appear which give some confidence in the simulated AEW patterns.

The link with SST patterns is not easy to establish for such integrated quantities but some global or regional SST features may be associated with large anomalies in the total variance, such as the 1982-83 El Niño event, the 1984 warm Gulf of Guinea SST anomaly or the combined El Niña/Warm Gulf of Guinea pattern in 1988. The 1979 large total variance does not seem to be related to any particular SST pattern. To define more objectively the association between AEW and SST, two indices were constructed to characterise the two components of the dipole structure, seen in Figure 6, by averaging the first MMP over the Sahelian and Guinean regions. The domain covering the Sahelian region extends from 20°W to 10°E, 16 to 24°N and the domain covering the Guinean region extends from 10°W to 20°E, to 5 to 13°N. These domains have been chosen so that maximum negative and positive anomalies observed in Figure 6 are roughly centred. For the robustness of the results, the two indices were averaged over the 10 members of each year. Correlations between the two indices and seasonal (JJAS) SST field over the period 1979-1993 are statistically significant (above the 95% threshold) over a broad region of the tropical Atlantic Ocean with negative values for the Sahelian region and positive values for the Guinean region (Figure 7). This corresponds to a southward (northward) displacement of the maximum wave amplitude in the first MMP in years with a warm (cold) tropical Atlantic anomaly, showing that equatorial Atlantic SST anomalies play a dominant role in the modulation of AEW in the ARPEGE GCM simulations. Remote teleconnections between AEW activity and SST in other oceans are weaker and less structured than Atlantic correlations. In ERA15, the first MMP does not show any clear link with SST (not shown), except between the Guinean index and equatorial Indian Ocean or the Sahelian index and West Atlantic Ocean. Some correlations also exist with Pacific SST without any clear pattern.

The periods of AEW are between 5 and 5.5 days, except for the year 1993 which has a period of 4.78 days for the first MMP. Interannual variability of the periods does not seem to present a coherent structure in relation with variance modes. Some particular years emerge but without apparent links with boundary forcings. In addition, there is no apparent link between periods and SST anomalies, and error bars are large while the mean values do not fluctuate so much. Periods of the first two MMPs, in ERA15, show some interannual variability but extreme years do not correspond to strong global SST patterns.

5. Intraseasonal variability of the modes

In addition to the spatial patterns the CEOF analysis gives also the temporal variation of the leading modes over the 123 days of the analysis. The modulus of the first two complex EOF gives information on the evolution of the amplitude of the AEWs over the June to September monsoon season. The 10 members available for each year allow to estimate the stability of the amplitude patterns. The average over the 10 members for CEOF-1 shown as the central solid continuous line in Figure 8a represent the mean seasonal evolution of the AEW activity. The maximum activity generally occurs during August in association with the northward penetration of the monsoon flow. It can be noticed that the years with maximum intensity of

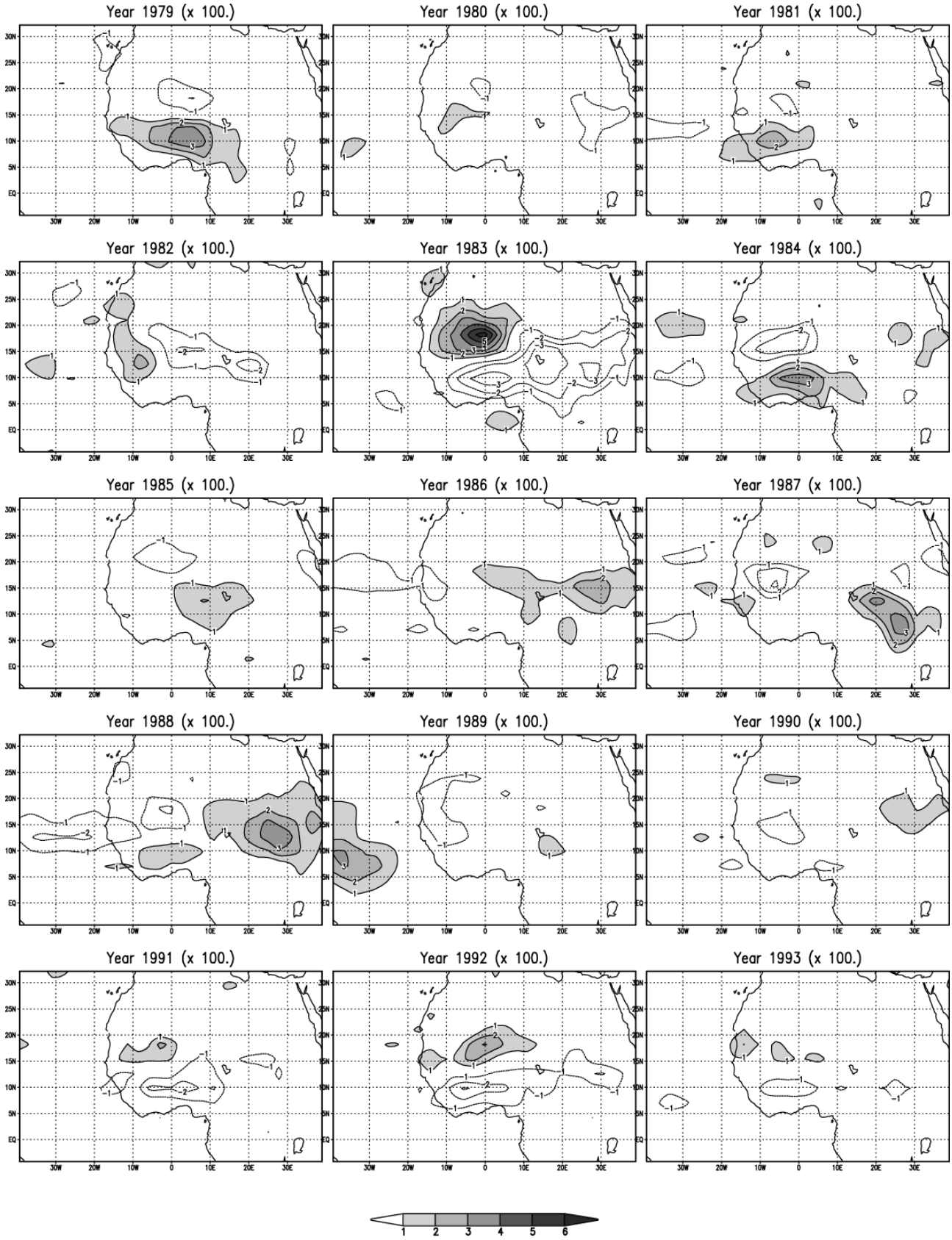

Figure 6: Interannual ensemble-mean anomalies of first CEOF amplitude with respect to total 15 year mean (150 runs). Contour interval: 10^{-2}.

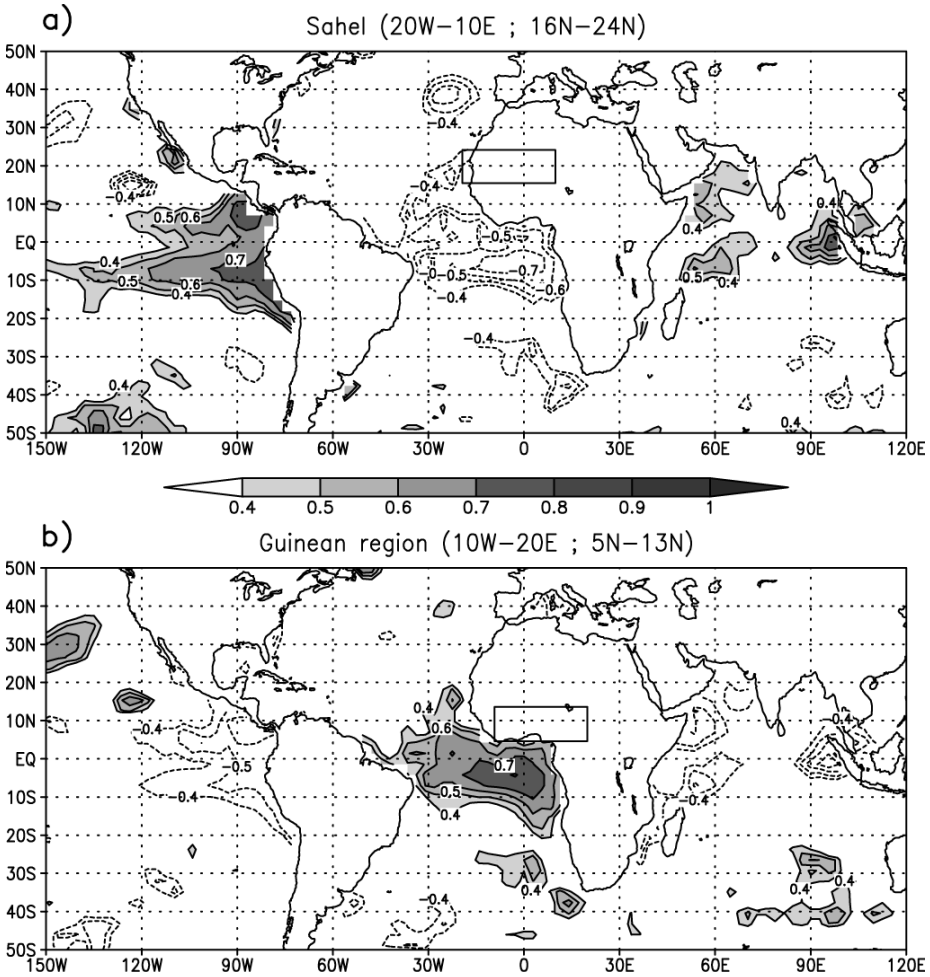

Figure 7: 15-years correlation between a) Sahelian and b) Guinean first CEOF amplitude averages and JJAS averaged SST over 1979 to 1993 for control experiment. Contour interval of 0.1 when absolute value of correlation is greater than 0.4 (This corresponds approximately to the 95 significant level (0.51) for the correlation coefficient).

mode-1 amplitude (Figure 4) and southward displacement of the maximum amplitude (Figure 6) such as 1984, 1985, 1986, 1988 and 1989 have a well defined seasonal evolution with a prominent peak in August. On the other hand, years with the smaller CEOF-1 amplitude and northward position (1982, 1983, 1991, 1992, 1993) tend to have a rather flat seasonal evolution. The first CEOF is thus capable of discriminating not only the geographical position of the AEW tracks among the different years but their specific seasonal differences as well. A similar pattern is not readily apparent in the ERA15 CEOF-1 amplitude (Figure 8b) in which such the possible underlying tendency of the seasonal cycle seems completely masked by the large intraseasonal fluctuations. Such fluctuations are also present in each of the 10 individual members of the GCM simulation and a measure of their amplitude is provided by the spread on each side of the mean as illustrated by their standard deviation, maximum and minimum values. The intraseasonal fluctuations in ERA15 have clearly a low frequency component with periods of the order of 20 days or more as seen by counting the number of maxima occurring during the 123-day interval.

To quantify more precisely the frequencies of the intraseasonal modulation of the CEOF-1 amplitude a simple spectral analysis by the periodogram method has been applied to its time series, after removal of the mean seasonal evolution computed over the 15 years. The spectra shown in Figure 9 confirm the presence of low-frequency modulations with spectral peaks at periods in the range 20 to 60 days. However the position of the peaks vary in each ensemble member from the same year, and thus the average spectrum obtained for each year from the 10 simulations gives only an indication of an increase of variance at lower frequencies.

The years with higher CEOF-1 variance tend to have more prominent spectral peaks than the years with lower variance, at least for the GCM simulations.

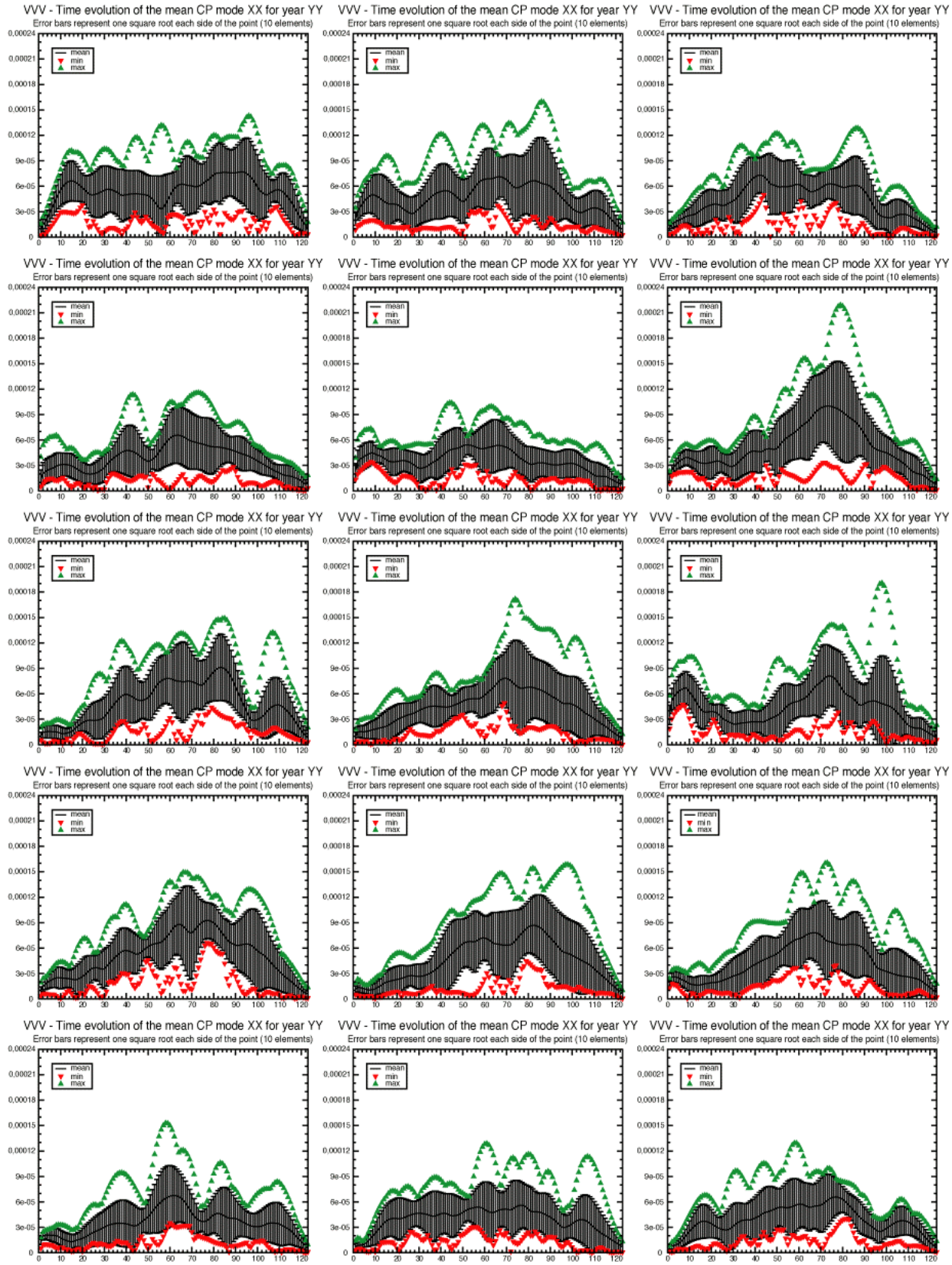

Figure 8: Interannual variability of first CEOF amplitude of filtered 850 hPa vorticity. a) for 10-ensemble GCM simulation. Bars represent one standard deviation each side of the mean. Triangle pointing up and down are maximum and minimum of the 10 elements.

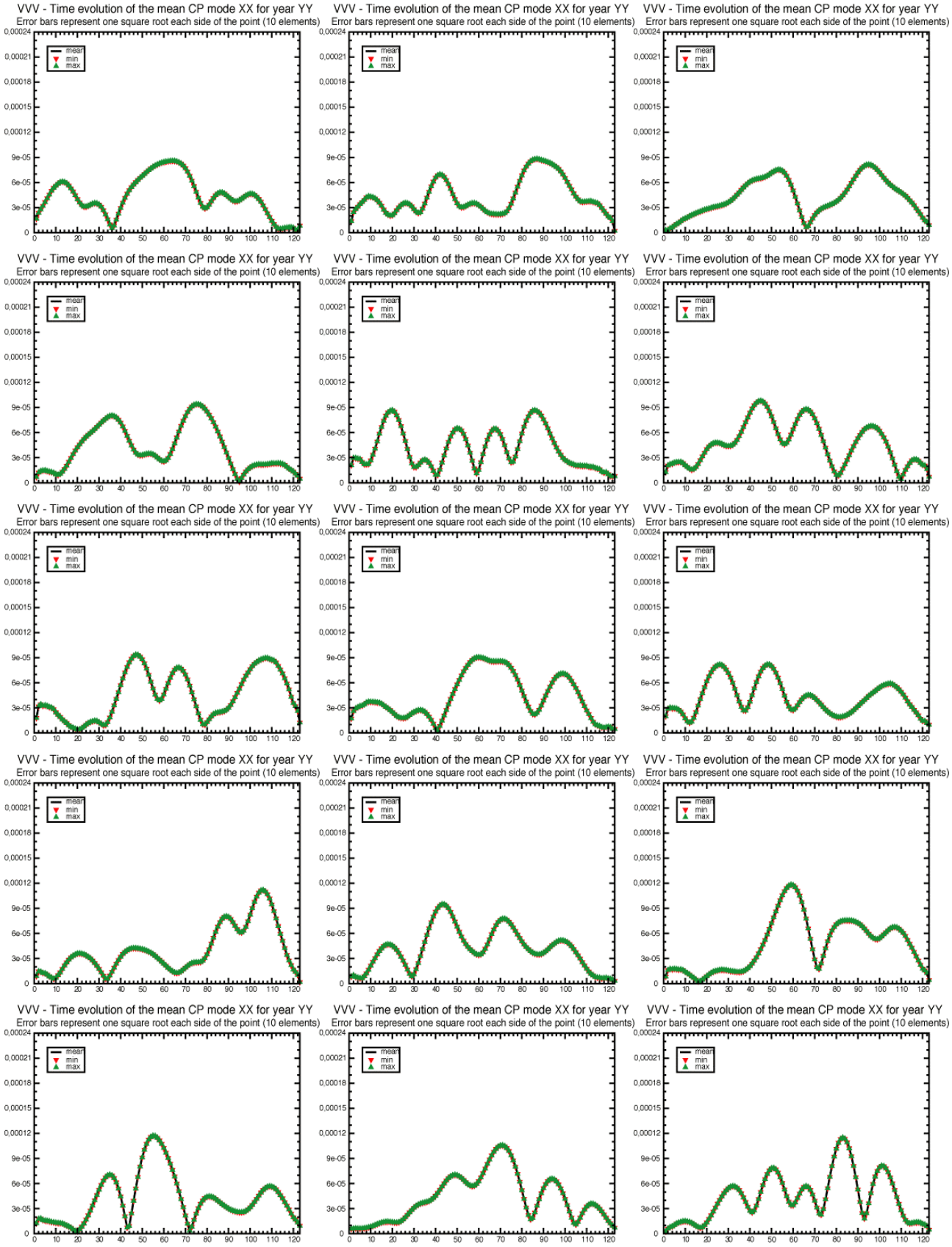

Fig 8b Interannual variability of first CEOF amplitude of filtered 850 hPa vorticity forERA15.

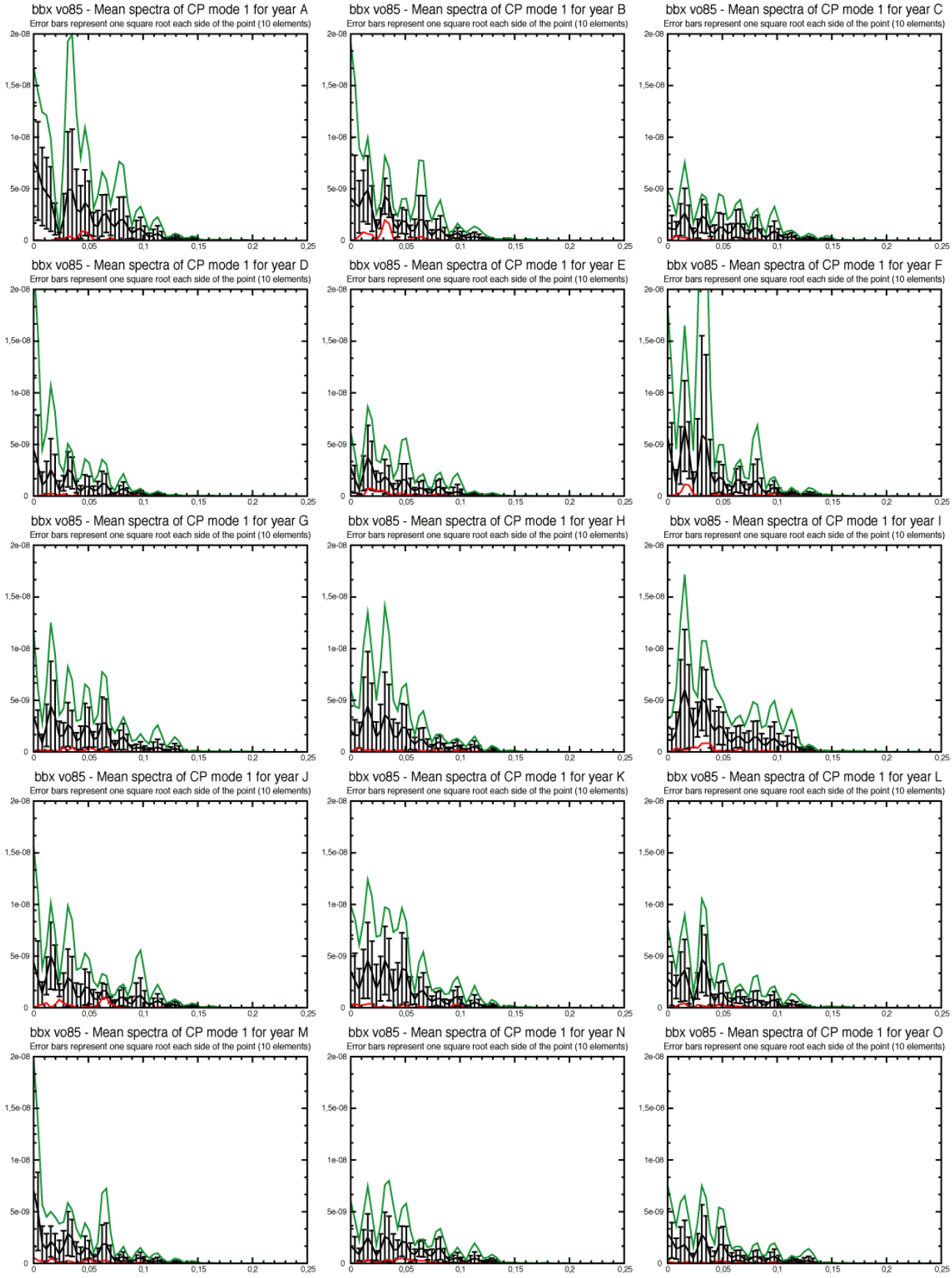

Figure 9 Interannual variability of spectra of first CEOF amplitude of filtered 850 hPa vorticity. a) for 10-ensemble GCM simulation. Bars represent one standard deviation each side of the mean. Triangle pointing up and down are maximum and minimum of the 10 elements.

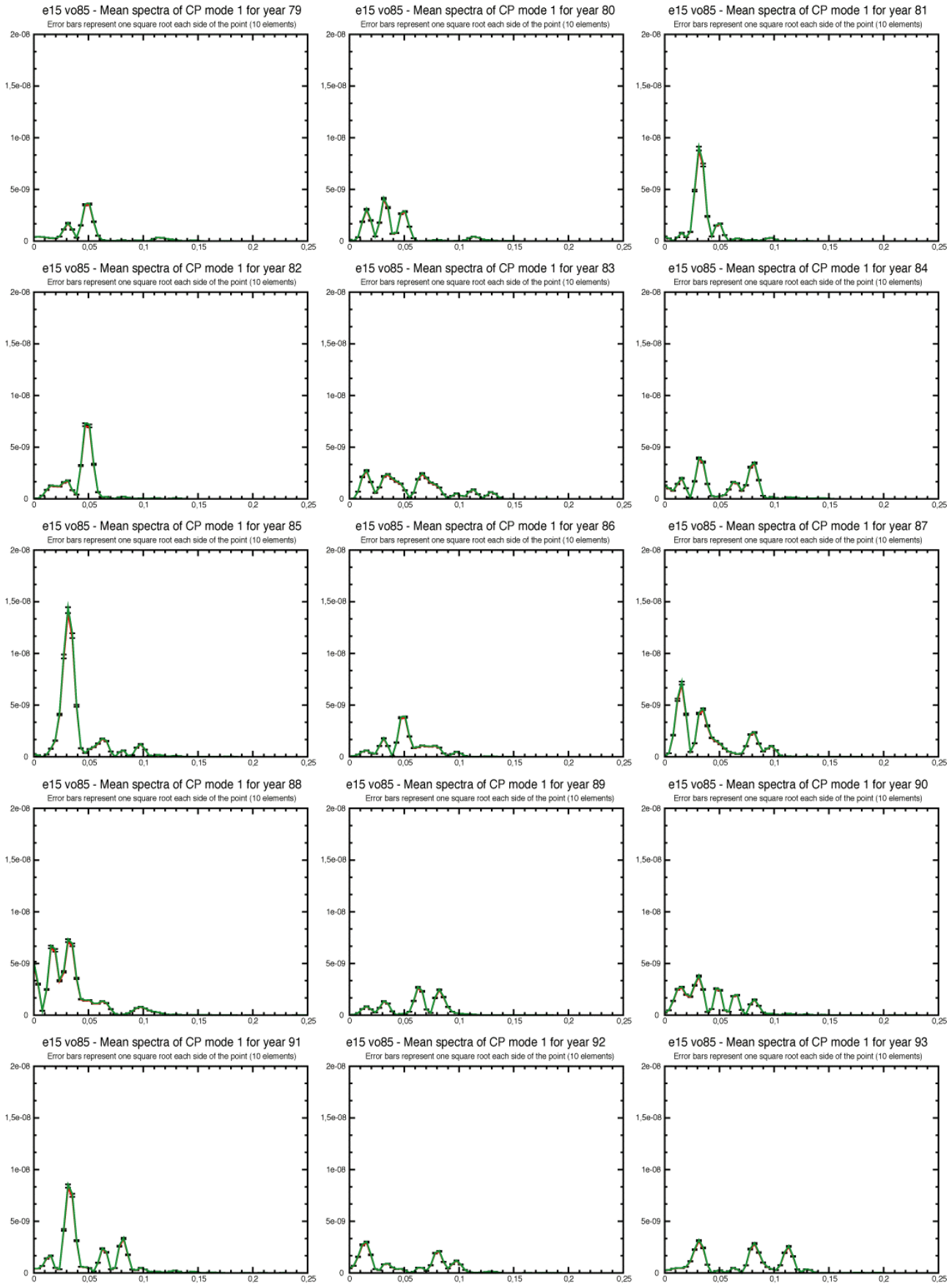

Figure 9 b) Same as Figure 9a for ERA15

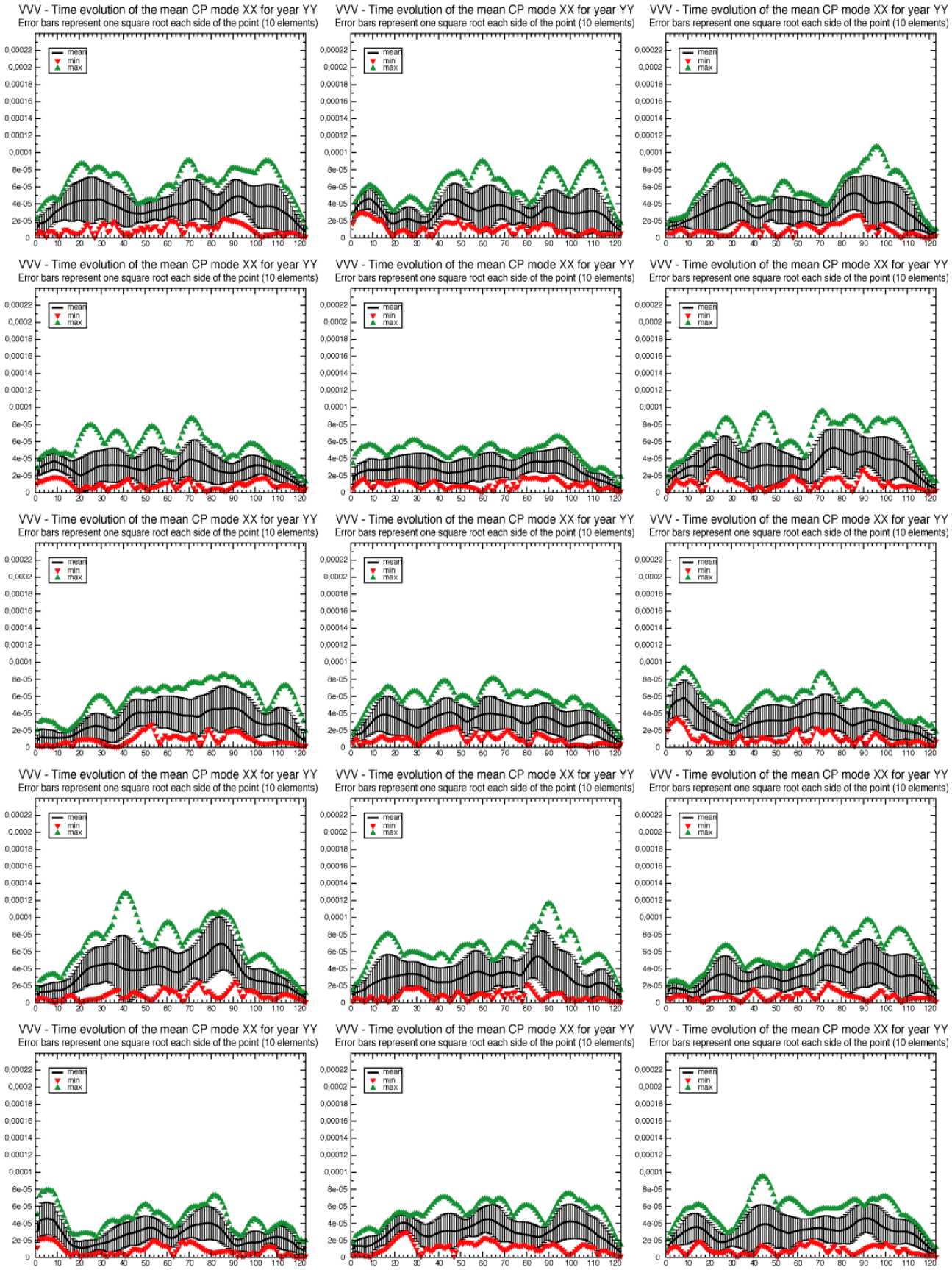

Figure 10a Same as Figure 8a for CEOF-2 amplitude

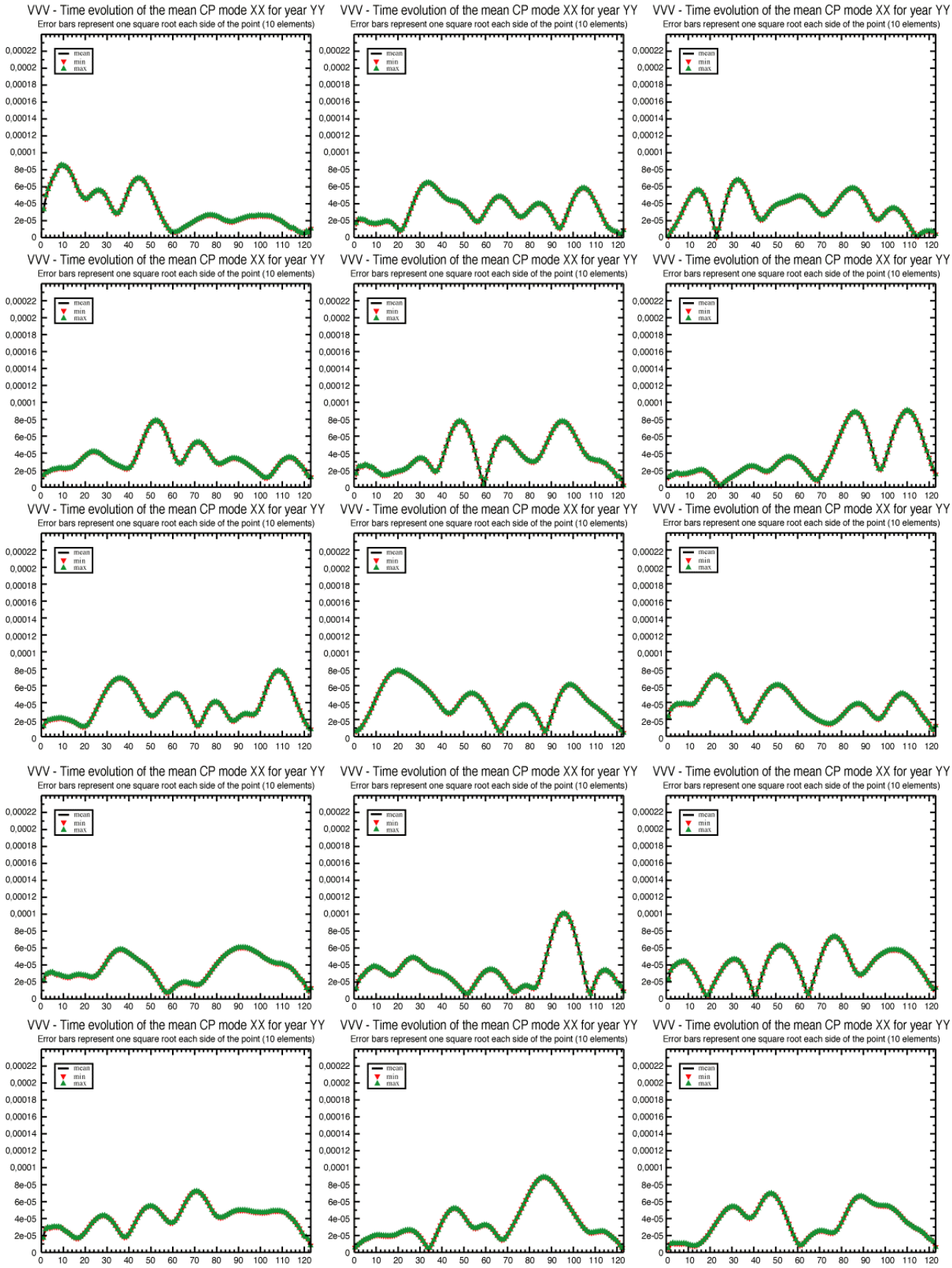

Fig 10b Same as Figure 8b for CEOF-2 amplitude

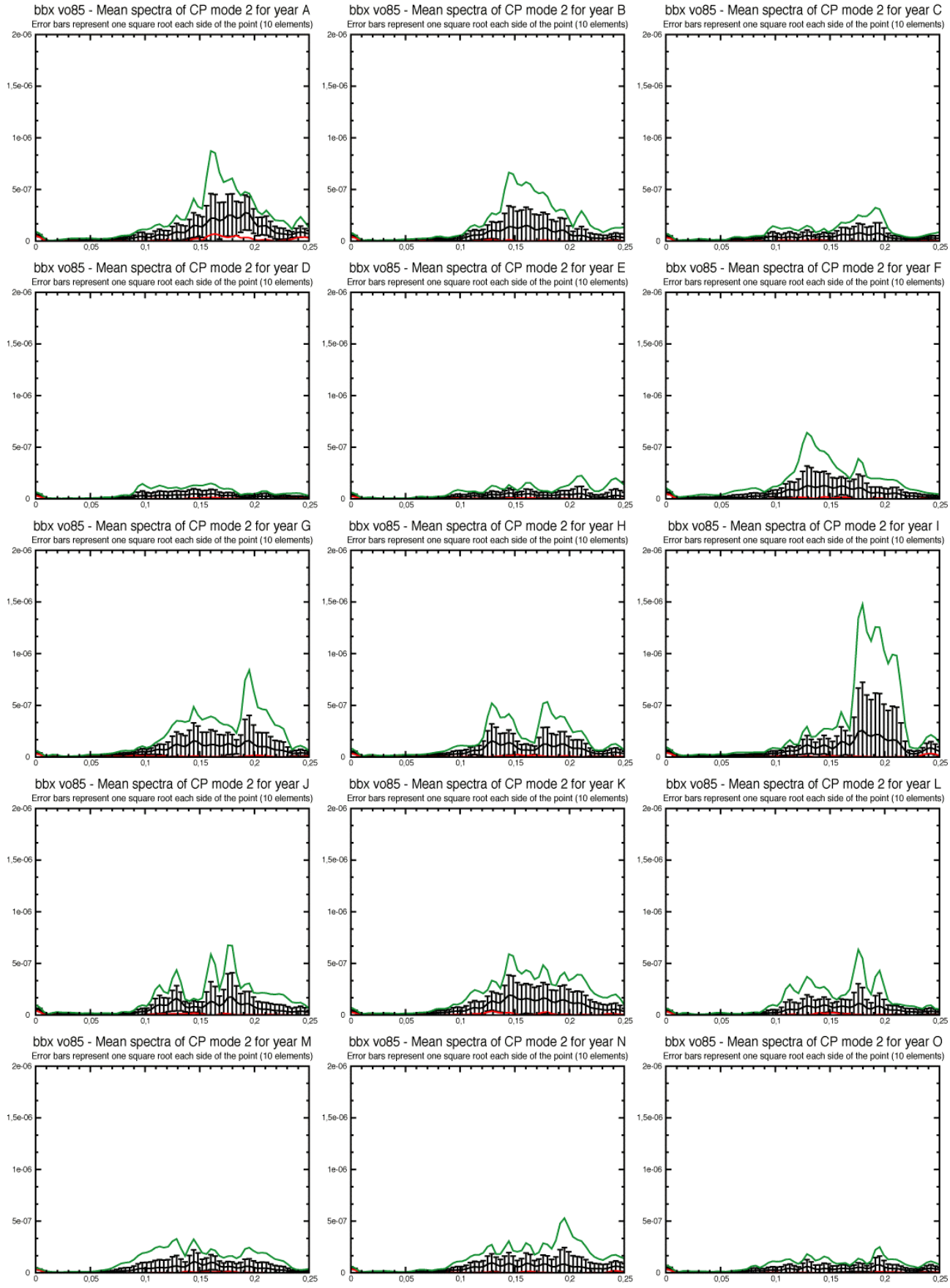

Figure 11 Same as Figure 9a for CEOF-2 amplitude

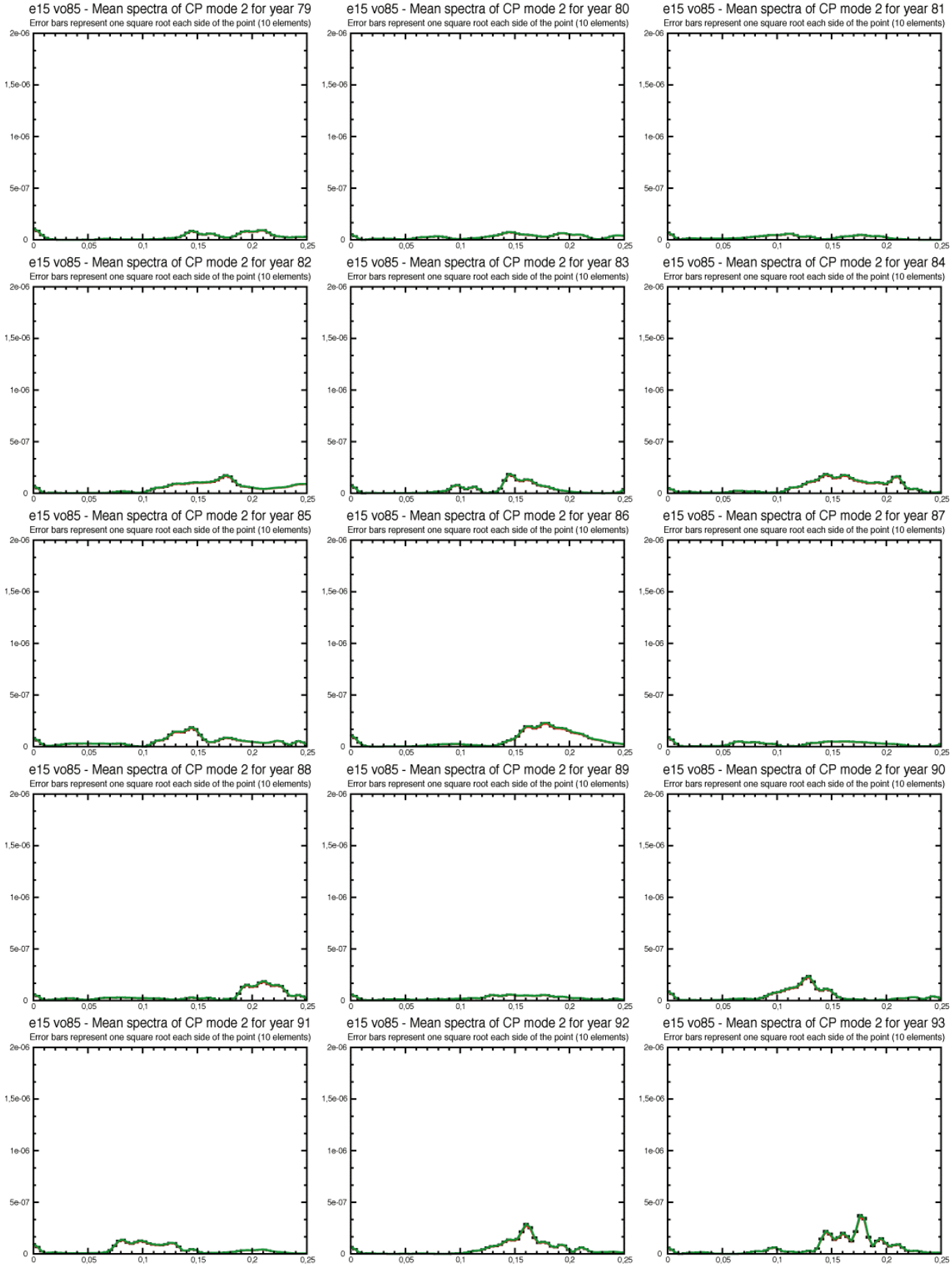

Figure 11b Same as Figure 9b for CEOF-2 amplitude

A similar analysis has been repeated for CEOF-2. The seasonal evolution seems less well defined than for CEOF-1 (Figure 10), and the intraseasonal fluctuations to be of higher frequency. This is confirmed by the

spectra (Figure 11) that show mostly a broad spectral peak in the range of 5 to 10 days. This shows that the CEOF analysis is efficient at separating two modes with very different spectral characteristics. A relationship between the seasonal evolution or spectra of CEOF-2 and its total variability (Figure 4) is not apparent

6. Discussion

Application of CEOF methods to analyse AEW has allowed to identify the interannual variability of the spatial distribution of the wave activity. The two modes isolate significant interannual variability in two separate areas. The first mode of variability (CEOF-1) shows correlations with SST patterns in the tropical Atlantic, with warm anomalies generally associated to more southerly tracks of the AEWs. The temporal distribution of the CEOF amplitude shows a seasonal variation with a maximum in August for CEOF-1. Considerable low-frequency intraseasonal modulation of the AEW variability is found, as well as interannual variability of the seasonal and intraseasonal evolution. A spectral analysis of the intraseasonal variability confirms the very different spectra of CEOF-1 and CEOF-2: a red noise background with peaks with periods in the range 20 to 60 days for CEOF-1, and a broad maximum from 5 to 10 days for CEOF-2. Possible developments and improvements of the analysis method could involve a rotation of the CEOFs, a different aggregation of the modes, and improved methods for their spectral analysis. A more detailed study of the intraseasonal fluctuations of the modes needs to be undertaken to investigate the possible associations of AEWs variability with the monsoon circulation over Africa (AEJ, TEJ, ZCIT, precipitation), or with Atlantic hurricanes (Landsea and Gray, 1992). The low-frequency variability of CEOF-1 in the range 20 to 60 days invites to investigate its possible links with the MJO. Another important topic which may need to be considered is the possible impact of soil moisture on the evolution of AEW activity.

Acknowledgments: We thank Jean-Pierre Céron and Jean-François Guérémy for their statistical analysis software package and help. This study has been supported by a grant from the European Commission Fifth Framework Programme (PROMISE contract EVK2-CT-1999-00022) and by the French Programme National d'Etude de la Dynamique du Climat (PNEDC). The figures have been drawn with GrADS software (http://grads.iges.org/grads/).

References

Bougeault P (1985) A simple parameterization of the large-scale effects of cumulus convection. *Mon Weather Rev* **113**: 2108-2121

Burpee RW (1972) The origin and structure of easterly waves in the lower troposphere of North Africa. *J Atmos Sci* **29**: 77-90

Céron JP, Guérémy JF (1999) Validation of the space-time variability of African easterly waves simulated by the CNRM GCM. *J Climate* **12**: 2831-2855

Céron, JP, Guérémy JF, Sarr A (2001): African monsoon synoptic variability: Validation of the Météo-France GCM. *Phys. Chem. Earth* (B) **26**: 149-153

Chen YL, Ogura Y (1982) Modulation of convective activity by large-scale flows patterns observed in GATE. *J Atmos Sci* **39**: 1260-1279

Déqué M, Dreveton C, Braun A, Cariolle D (1994) The ARPEGE/IFS atmosphere model: A contribution to the French community climate modelling. *Climate Dyn* **10**: 249-266

Diedhiou A, Janicot S, Viltard A, de Felice P (1998) Evidence of two regimes of easterly waves over West Africa and the tropical Atlantic. *Geophysical Research Letters* **25**: 2805-2808

Diedhiou A, Janicot S, Viltard A, de Felice P, Laurent H (1999) Easterly wave regimes and associated convection over West Africa and tropical Atlantic: Results from the NCEP/NCAR and ECMWF reanalyses. *Climate Dyn* **15**: 795-822

Douville H, Royer JF, Mahfouf JF (1995) A new snow parametrization for the Météo-France climate model. Part I: Validation in stand-alone experiments. *Climate Dyn* **12**: 21-35

Douville H, Royer JF, Mahfouf JF (1995) A new snow parametrization for the Météo-France climate model. Part II: Validation in a 3-D GCM experiment. *Climate Dyn* **12**: 37-52

Douville H (2003) Assessing the influence of soil moisture on seasonal climate variability with AGCMs. *Hydrometeorology* (in press)

Druyan LM, Hall TM (1994) Studies of African wave disturbances with the GISS GCM. *J Climate* **7**: 261-276

Estoque MA, Shukla J, Jiing JG (1983) African wave disturbances in a general circulation model. *Tellus* (Ser A) **35**: 287-295

Fontaine, B., S. Janicot and V. Moron, 1995: Rainfall anomaly patterns and wind field signals over West Africa in August (1958-1989). *J. Climate*, **8**, 1503-1510.

Fyfe JC (1999) Climate simulations of African easterly waves. *J Climate* **12**: 1747-1769

Garric G, Douville H, Déqué M (2002) Prospects for improved seasonal predictions of monsoon precipitation over Sahel. *Int J Climatol* **22**: 331-345

Gates WL (1992) AMIP: The Atmospheric Model Intercomparison Project. *Bull Amer Meteorol Soc* **73**: 1962-1970

Geleyn JF, Bazile E, Bougeault P, Déqué M, Ivanovici V, Joly A, Labbé L, Piédelièvre JP, Piriou JM, Royer JF (1995) Atmospheric parameterization schemes in Meteo-France's Arpege NWP model. *ECMWF Seminar Proc Parametrization of Sub-grid Scale Physical Processes*: 385-402

Gibson JK, Kallberg P, Uppala S, Hernandez A, Nomura A, Serrano E (1997) ERA description. *ECMWF Reanalysis Project Report* n° 1, 72 pp

Goulet L, Duvel JP (2000) A new approach to detect and characterize intermittent atmospheric oscillations: Application to the intraseasonal oscillation. *J Atmos Sci* **57**: 2397-2416

Hamming RW (1977) *Digital Filters*. Prentice-Hall, Englewood Cliffs, NJ, 226 pp

Hayashi Y (1977) On the coherence between progressive and retrogressive waves and a partition of space-time power spectra into standing and traveling parts. *J Appl Meteorol* **16**: 368-373

Hayashi Y (1979) A generalized method of resolving transient disturbances into standing and traveling waves by space-time spectral analysis. *J Atmos Sci* **36**: 1017-1029

Hayashi Y (1982) Space-time spectral analysis and its applications to atmospheric waves. *J Meteorol Soc Japan* **60**: 156-171

Horel JD (1984) Complex principal component analysis: Theory and examples. *J Climate Appl Meteorol* **23**: 1660-1673

Landsea CW, Gray WM (1992) The strong association between western Sahelian monsoon rainfall and intense Atlantic hurricanes. *J Climate* **5**: 435-453

Louis JF, Tiedtke M, Geleyn JF (1981) A short history of the operational PBL parameterization at ECMWF. In: *Workshop on Planetary Boundary Layer Parameterization*, 25-27 November 1981. ECMWF, Reading, pp 59-80

Mahfouf JF, Manzi AO, Noilhan J, Giordani H, Déqué M (1995) The land surface scheme ISBA within the Météo-France climate model ARPEGE. Part I: Implementation and preliminary results. *J Climate* **8**: 2039-2057

Mahfouf JF, Noilhan J (1996) Inclusion of gravitational drainage in a land surface scheme based on the force-restore method. *J Appl Meteorol* **35**: 987-992

Morcrette JJ (1990) Impact of changes to the radiation transfer parameterizations plus cloud optical properties in the ECMWF model. *Mon Wea Rev* **118**: 847-873.

Moustaoui M., J.F. Royer, F. Chauvin, 2002 : African easterly wave activity in a variable resolution GCM. *Climate Dynamics* **19**: 289-301.

Noilhan J, Planton S (1989) A simple parameterization of land surface processes for meteorological models. *Mon Weather Rev* **117**: 536-549

Reed RJ, Norquist DC, Recker EE (1977) The structure and properties of African wave disturbances as observed during Phase III of GATE. *Mon Weather Rev* **105**: 317-333

Reed RJ, Klinker E, Hollingsworth A (1988) The structure and characteristics of African easterly wave disturbances as determined from the ECMWF operational analysis/forecast system. *Meteorol Atmos Phys* **38**: 22-33

Ricard JL, Royer JF (1993) A statistical cloud scheme for use in an AGCM. *Ann Geophys* **11**: 1095-1115

Thorncroft CD, Rowell DP (1998) Interannual variability of African wave activity in a general circulation model. *Int J Climatol* **18**: 1305-1323

Wallace JM, Dickinson RE (1972) Empirical orthogonal representation of time series in the frequency domain. Part I: Theoretical considerations. *J Appl Meteorol* **11**: 887-892